



The Current Martian Crater Production Function

I. J. Daubar (1), A. S. McEwen (1), S. Byrne (1) and M. Kennedy (2)
(1) Lunar & Planetary Laboratory, University of Arizona, Tucson, AZ, 85721 (ingrid@lpl.arizona.edu)
(2) Malin Space Science Systems, P.O. Box 910148, San Diego, CA, 92191

Abstract

Discoveries of recent, dateable impacts establish the present-day cratering rate on Mars. They allow us to evaluate crater-dating models and clarify the effectiveness of using small craters to date small areas and/or geologically recent terrains. Although the current impact rate may not be representative of geologic time or all impactor sizes, it is a definitive measurement that can be compared to models.

1. Background

Malin et al. [8] reported finding 20 new impact sites using the Mars Orbital Camera, 19 of which the High-Resolution Imaging Science Experiment (HiRISE) has confirmed as new. Since then, the Mars Reconnaissance Orbiter has provided repeated coverage at medium resolution with the Context (CTX) camera, plus high-resolution follow-up imaging with HiRISE. This method has thus far revealed an additional 182 new impact sites with incredible variety and detail. Progress has previously been reported in [1-3, 5-7, 9].

2. Detection of new impact sites

New martian impact sites are recognized in CTX data as dark spots caused by the disturbance of surrounding high-albedo dust primarily by the impact airburst – spots which are not present in previous data (CTX or various other, older data sets). The HiRISE camera then follows up to confirm an impact origin. This method requires a surface covering of dust, so discoveries are almost all limited to the dustiest regions of Mars [Fig. 1].

3. Description of new impact sites

The number of confirmed new impact sites has reached 201 as of the last observations taken before the 2011 solar conjunction (not including several with no identifiable craters, interpreted to be recent

airbursts or sites of localized aeolian darkening). A slight majority (57%) of these are “cluster” sites with multiple craters formed by the breakup of the impactor in the martian atmosphere.

Measured new crater diameters range from several to ~50 meters. We calculate effective diameters for clusters of multiple craters as $D_{\text{eff}} = (\sum D^3)^{1/3}$ [6, 8]. Individual craters within those clusters range from smaller than HiRISE can resolve to tens of meters.

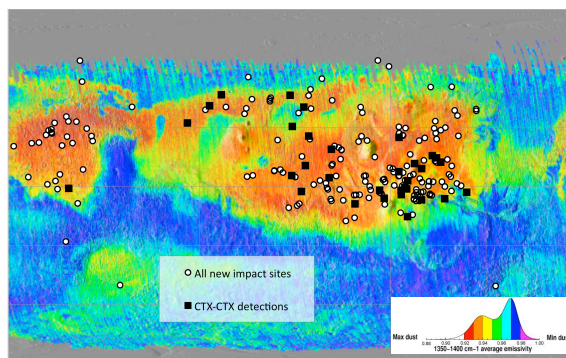


Fig. 1: Global TES dust cover index map [11] showing locations of 201 dated impact sites on Mars. The majority of sites are in areas of high dust cover.

4. Production Function

The production function is normally expressed as the number of new craters in a given diameter range per square kilometer per year. In order to compare the current rate of impacts to such a theoretical function, an area to which to scale the size-frequency distribution is required. Typically in crater counting, this would be the area over which all craters were counted. However, due to the detection bias of our method as well as limited data coverage, new craters are not detected over the entire martian surface, and may not be dateable if prior imaging was poor. In order to get the most robust estimate of the current impact rate, we limit the data set to those craters whose formation dates are constrained solely by CTX data. This ensures consistency in data quality, as well as completeness, since every new CTX image of

dusty regions has been examined for dark spots that resemble new impact sites.

The number of craters in a given diameter size bin is then scaled by a composite area-time factor (ATF), which represents the sum of all overlap area between CTX images, multiplied by the time elapsed between a given pair of overlapping images:

$$ATF = \sum_i a_i \Delta t_i \quad (1)$$

Here a_i is the overlap area (km^2) of the i^{th} possible pair of CTX images, Δt_i is the elapsed time between those two images, and the sum is performed over all possible pair combinations of CTX images in the dusty regions. These were defined as having an average value of TES emissivity [11] over the image footprint of <0.95 . CTX images poleward of 60° latitude were excluded; no new impact detections have been made at those latitudes, where albedo patterns are reset yearly. The result of dividing the SFD of new craters by this factor is the number of new craters per area per time, *i.e.* the production function.

5. Results

The new crater impact SFD scaled by the area-time factor is shown in Fig 2. The rollover at small sizes could be a resolution effect and/or the result of atmospheric ablation at small sizes, especially small fragments from atmospheric breakup that forms clusters. The Hartmann 2005 cratering production function [4], extended down to these small sizes, falls within the error bars of the data. (This PF is similar to that of [10] at these diameters, with a downward correction for atmospheric loss.) However, this may be fortuitous if the current impact rate is not typical of geologic time, e.g. the last few millions of years that the models represent. Our SFD is somewhat shallower than Hartmann's PF, but this is not yet a statistically convincing result.

Despite the encouraging agreement between this model prediction and observations, caution should still be applied when attempting to apply model ages to older surfaces using small craters. Firstly, this is a population of known primaries, so any potential secondary contamination in the observations is automatically excluded. Secondly, we have the ability to identify clusters of craters resulting from a

single impact event, whereas an examination of the same scene without the unifying dark spot might result in craters within a cluster being mistaken for individual primaries, dramatically steepening the slope of the SFD and artificially increasing the resulting model age.

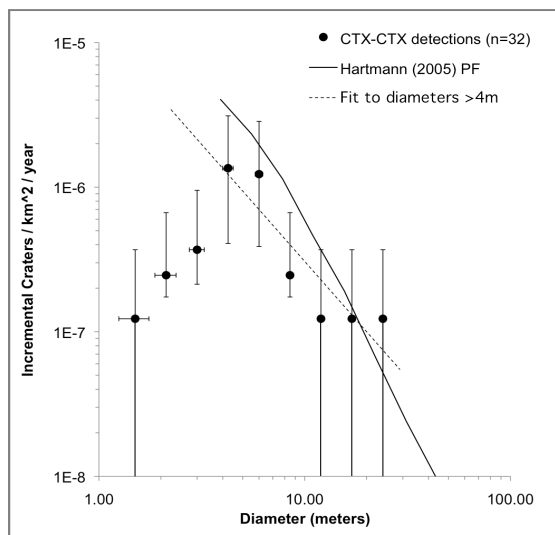


Fig. 2: Size-frequency diagram of new impact effective diameters scaled by ATF, compared to the Hartmann 2005 [4] production function. Also shown is a least-squares fit to crater diameters >4 meters, showing a slightly shallower slope than the model PF.

References

- [1] Daubar I. J. and McEwen A. S. (2009) *LPSC XL*, Abs. 2419.
- [2] Daubar I. J. *et al.* (2010) *LPSC XLI*, Abs. 1978.
- [3] Daubar I. J. *et al.* (2011) *LPSC XLII*, Abs. 2232.
- [4] Hartmann W. K. (2005) *Icarus*, 174, 294-320.
- [5] Ivanov B. A. *et al.* (2008) *LPSC XXXIX*, Abs. 1402.
- [6] Ivanov B. A. *et al.* (2009) *LPSC XL*, Abs. 1410.
- [7] Kennedy M. R. and Malin M. C. (2009) *AGU Fall Meeting*, Abs. ID P43D-1455.
- [8] Malin M. C. *et al.* (2006) *Science*, 314, 1573-1577.
- [9] McEwen A. S. *et al.* (2007) *LPSC XXXVII*, Abs. 2009.
- [10] Neukum G. *et al.* (2001) *Space Sci. Rev.*, 96, 55-86.
- [11] Ruff S. W. & Christensen P. R. (2002) *JGR*, 107, 5127.